Near edge X-ray absorption mass spectrometry on coronene

Reitsma, G.; Boschman, L.; Deuzeman, M. J.; Hoekstra, S.; Hoekstra, R.; Schlatholter, T.

Published in:
Journal of Chemical Physics

DOI:
10.1063/1.4905471

Near edge X-ray absorption mass spectrometry on coronene

G. Reitsma, L. Boschman, M. J. Deuzeman, S. Hoekstra, R. Hoekstra, and T. Schlathölter

Citation: The Journal of Chemical Physics **142**, 024308 (2015); doi: 10.1063/1.4905471
View online: https://doi.org/10.1063/1.4905471
View Table of Contents: http://aip.scitation.org/toc/jcp/142/2
Published by the American Institute of Physics

Near edge X-ray absorption mass spectrometry on coronene

G. Reitsma,[1] L. Boschman,[1,2] M. J. Deuzeman,[1] S. Hoekstra,[3] R. Hoekstra,[1] and T. Schlathölter[1]
[1]*Zernike Institute for Advanced Materials, University of Groningen, Nijenborgh 4, 9747AG Groningen, The Netherlands*
[2]*Kapteyn Astronomical Institute, University of Groningen, Groningen, The Netherlands*
[3]*Van Swinderen Institute, University of Groningen, Groningen, The Netherlands*

(Received 19 August 2014; accepted 19 December 2014; published online 12 January 2015)

We have investigated the photoionization and photodissociation of free coronene cations $C_{24}H_{12}^{+}$ upon soft X-ray photoabsorption in the carbon K-edge region by means of a time-of-flight mass spectrometry approach. Core excitation into an unoccupied molecular orbital (below threshold) and core ionization into the continuum both leave a C 1s vacancy, that is subsequently filled in an Auger-type process. The resulting coronene dications and trications are internally excited and cool down predominantly by means of hydrogen emission. Density functional theory was employed to determine the dissociation energies for subsequent neutral hydrogen loss. A statistical cascade model incorporating these dissociation energies agrees well with the experimentally observed dehydrogenation. For double ionization, i.e., formation of intermediate $C_{24}H_{12}^{3+\star}$ trications, the experimental data hint at loss of H^+ ions. This asymmetric fission channel is associated with hot intermediates, whereas colder intermediates predominantly decay via neutral H loss. © *2015 AIP Publishing LLC.* [http://dx.doi.org/10.1063/1.4905471]

I. INTRODUCTION

The formation and stability of polycyclic aromatic hydrocarbons (PAHs) is of key relevance for many research fields ranging from astrochemistry[1] to combustion research.[2] In particular, gas-phase PAH interactions with energetic photons have been the subject of intense study because of the direct relevance of such processes in astrophysical environments[3] and because of the opportunities of PAH photoionization as a tool for analytical chemistry.[4]

In a series of pioneering experiments, using synchrotron radiation, Leach and coworkers have investigated vacuum ultraviolet (VUV) photoionization of a variety of gas-phase neutral PAHs by means of photoelectron-photoion coincidence spectroscopy[5,6] or by photoionization mass spectrometry.[7] Upon moderate excitation, PAH cations dissociate predominantly by neutral H atom, or H_2 loss, or by acetylene loss, with appearance photon energies increasing with PAH size. For instance, the appearance energy for H atom loss is 13.81 eV for benzene and 18.7 eV for coronene.[8] Note that direct loss of single C atoms from the PAH skeleton has so far only been observed in atomic collision experiments,[9,10] where the energy transfer to the C atom needs to exceed 25.5 eV.[11] For small systems such as benzene and naphthalene, appearance energies for H atoms and H_2 are similar, whereas, e.g., for coronene, H_2 loss requires about 1.4 eV more internal energy and acetylene loss is not observed at all.[8] Calculated absolute photoabsorption cross sections[12] for neutral PAHs and for their respective cations are in very good agreement with experimental data. For all PAH species studied, the VUV absorption spectrum is dominated by a broad continuum between 10 eV and 30 eV that peaks between 15 eV and 20 eV and that is quantitatively similar for ions and neutrals.

Upon UV or VUV photoionization, large astrophysically relevant PAHs such as coronene are subject to H atom or H_2 loss. However, these channels are outcompeted by non-dissociative ionization, by far. Inner-shell photoexcitation or photoionization involves larger excitation energies and accordingly opens up more fragmentation channels, e.g., successive H atom loss or H_2 loss. However, beyond the VUV range, experimental data on PAH photoionization are scarce. At the C K-edge, Hübner *et al.*[13] have performed a high resolution near edge X-ray absorption spectroscopy (NEXAFS) study on naphthalene and found evidence for a strong coupling between electronic transitions and vibronic excitations. Very recently, in a combined experimental and theoretical NEXAFS investigation of anthracene, Klues *et al.*[14] showed that final state relaxation effects due to excitations from localized hole states have to be taken into account for an accurate interpretation of the experimental data. The molecular response upon K-edge photoabsorption, i.e., PAH fragmentation, has not been investigated yet.

The investigation of neutral PAH molecules upon photoionization is experimentally straightforward because effusive targets can be produced by mere evaporation. It is notoriously difficult to study photoionization of ions because the traditional crossed beam or merged beam experiments require high intensity ion beams. To our knowledge, no such studies have been performed for PAHs yet. A complementary approach towards photoionization of PAH cations is the use of radiofrequency (RF) ion traps for collection of a sufficiently dense cationic target. In pioneering experiments, a commercial[15]

or a home-built tandem mass spectrometer[16] was interfaced with synchrotron beamlines to investigate photoionization and photofragmentation of large cationic biomolecules.

In a recent study, K-edge photoexcitation at a fixed energy of 285 eV was used to study the relaxation of highly excited superhydrogenated PAHs.[18] Here, we report on the first near edge X-ray absorption mass spectrometry (NEXAMS) study on a PAH cation, scanning the full K-edge absorption energy range (283-305 eV). The data were obtained by interfacing our apparatus with a soft X-ray beamline at the BESSY II synchrotron. By comparison of experimental data with quantum chemical calculations, it will be shown that the degree of dehydrogenation can be used to estimate the internal energy of the intermediate multiply ionized molecule. A statistical cascade model is used to correlate the dehydrogenation with branching ratios as a function of internal energy. Finally, strong indications for the transition from neutral H atom (or H_2) to H^+ (or H_2^+) loss in coronene trications will be presented.

Throughout this paper, the following terminology will be used to distinguish between different types of hydrogen loss: (i) "(n)H atom loss" to address the (sequential) loss of atomic H, (ii) "H_2 loss" to address the emission H in molecular form, (iii) "(n)H loss" or "dehydrogenation" describes loss of hydrogen in either atomic or molecular form, or any combination of those. The latter is mainly used in the description of the experimental results as the mass spectra do not allow us to distinguish between sequential emission of, for example, 2 H atoms or a H_2 molecule.

II. EXPERIMENTAL METHOD

The experiments were performed on the soft X-ray beamline U49/2-PGM1 at the BESSY II synchrotron facility (Helmholtz Zentrum Berlin, Germany) using our tandem mass spectrometer setup.[16] Briefly, a beam of coronene cations was produced by an electrospray ionization (ESI) source, phase space compressed in a RF ion funnel and further guided by a linear RF ion guide. The molecular cations were mass selected by a quadrupole mass analyzer and then trapped in a RF ion trap. The setup was operated in a pulsed mode and in order to reach sufficiently high target densities, each cycle started with an ion accumulation period of 400 ms. The ions were collisionally cooled within a volume with a diameter of about 400 μm in the center of the trap by using a helium buffer gas. Following accumulation, the buffer gas was pumped down during 200 ms after which the ions were exposed to the soft X-ray photons. The photon beam was pulsed by an optical shutter and monitored by a silicon p-n junction photodiode. The photon exposure time varied between 700 and 1800 ms, depending on the ionization/fragmentation cross section for a specific photon energy. After each photon exposure period, a second helium buffer gas pulse was applied to collisionally cool energetic fragments. The trap potential well is typically 10 eV deep. This is sufficiently deep to trap PAH fragments, which have typical kinetic energies of 2-3 eV.[17] The trap content was extracted to a linear time-of-flight (TOF) mass spectrometer ($\frac{M}{\Delta M} \approx 300$) and detected on a micro channel plate (MCP) detector. The detector signal was processed by a 1 GHz digitizer.

In order to accurately quantify the net effect of the photon beam on the target molecules, two additional data cycles were performed for each spectrum. To obtain the contribution from the photoionization of the residual gas, a mass spectrum was recorded for an empty trap (ESI-off/photons-on). The initial trap content was determined by extraction of the trap content into the TOF spectrometer, without prior photon exposure (ESI-on/photons-off). The helium buffer gas was applied in all three cycles. The net effect of the photons on the target was then obtained by subtracting the ESI-off/photons-on spectrum and the ESI-on/photons-off spectrum from the main spectrum.

The coronene molecules were purchased from Sigma Aldrich (Germany) and were of $\geq$ 99% purity. Coronene cations were produced by adding 50 μl of 10 mM $AgNO_3$ to 1 ml saturated solution of coronene in ethanol, which leads to the following reaction: $C_{24}H_{12} + Ag^+ \longrightarrow Ag(s) + C_{24}H_{12}^+$. The solution was then pumped through the ESI needle at a 0.2 ml/h flow rate. For the natural ^{13}C isotope abundance of 1.1%, the abundance of singly isotopic coronene at $\frac{m}{q} = 301$ is 20% and the abundance of doubly isotopic coronene at $\frac{m}{q} = 302$ is 3%.

The TOF mass spectrum was calibrated by fixing the $C_{24}H_{12}^+$ parent peak at $\frac{m}{q} = 300$ and the two stable silver isotopes at $\frac{m}{q} = 106.9$ and 108.9. Low mass fragments are not visible in the mass spectra as the ion trap has a low-mass cut-off around $\frac{m}{q} = 50$. The ion yield was normalized to the exposure time, the photon flux, and the intensity of the parent peak. The quantum efficiency of the photodiode was assumed to be constant over the limited range of photon energies (283-305 eV).

A NEXAMS spectrum is the normalized photoionization/photodissociation product yield as a function of the photon energy. We extracted NEXAMS spectra from mass spectra recorded over the photon energy range from 283 to 305 eV. The stepsize was adjusted to the anticipated spectral features, varying from 0.25 eV up to a few eV at an energy resolution of 150 meV.

III. RESULTS AND DISCUSSION

A. General features of the mass spectra

The initial electronic processes that occur upon coronene near C K-edge photoabsorption are summarized in Figure 1. Generally speaking, two sequences can be distinguished above and below ionization threshold. For photon energies above the ionization threshold, ionization of the $C_{24}H_{12}^+$ parent ion

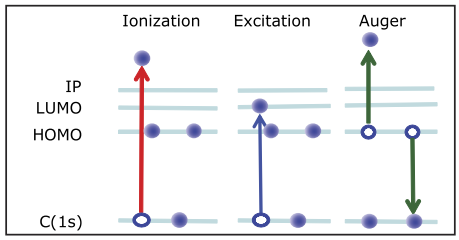

FIG. 1. Schematic representation of the relevant processes for K-edge photoabsorption. Abbreviations: Ionization Potential (IP), Highest Occupied Molecular Orbital (HOMO), and Lowest Unoccupied Molecular Orbital (LUMO).

leads to formation of $C_{24}H_{12}^{2+}$. Subsequently, the K-hole gets filled by an Auger decay and the emission of an Auger electron leaves $C_{24}H_{12}^{3+}$ trications. Below the ionization threshold, instead of an ionization, initially the 1s electron gets excited to an unoccupied molecular orbital. The subsequent Auger decay here increases the charge state by one, leading to the formation of $C_{24}H_{12}^{2+}$ dications. Note that in the following, the terms, dication and trication, will be used to address all doubly and triply charged ions, independent of the degree of dehydrogenation.

In Figure 2, six mass spectra are displayed which were taken after absorption of photons with energies 285, 288, 290.5, 293.5, 295, and 300 eV. The main spectral features shift from dications, $\frac{m}{q} = 146 - 150$ (blue lines), to trications, $\frac{m}{q} = 98 - 100$ (red lines), when crossing the ionization threshold. Both the dications and the trications show a distribution of peaks due to H loss. This dehydrogenation strongly depends on the amount of energy which is deposited into the molecule.

The mass spectrum has some further features at $\frac{m}{q} = 85$, 86, 87, 109, 110, 111, 120, 121, 122, 123, 124, 132, 133, 134, 135, and 136 which can be assigned to $C_nH_m^+$ type fragments. The intensity of these fragments increases with increasing photon energy.

B. NEXAMS spectra

Figure 3 displays the NEXAMS spectra for dications and trications. These spectra can be compared with previously published NEXAFS data on coronene[19] and smaller PAHs.[14,20,22] In contrast to NEXAFS data, where the total photoabsorption yield is directly recorded without any distinction between subsequent molecular response channels, NEXAMS is an action spectroscopy technique in which ion yields are the observables for photoabsorption. In general, a PAH absorption

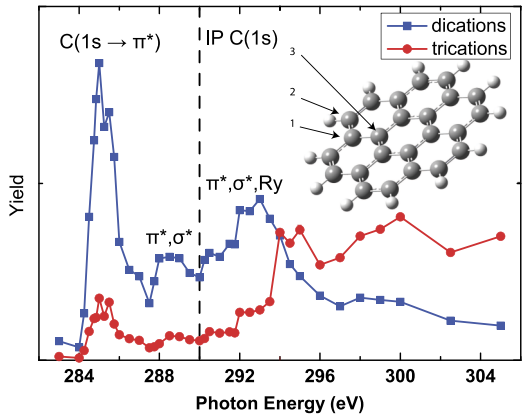

FIG. 3. NEXAMS spectra of the coronene dications (blue) and trications (red). The dashed line represents the ionization threshold for neutral coronene (see text). The inset shows the structure of a coronene molecule (figure produced by Ref. 37). The different atom types are labeled 1-3.

spectrum is affected by three main parameters: (i) the density of unoccupied states, (ii) energetic shifts of the C 1s energy, due to differences in chemical environment (≈ 0.5 eV), and (iii) the core-hole effect (several eV's). The dication spectrum has a strong resonance around 285 eV which originates from a $1s \longrightarrow \pi^*$ transition. This peak has an internal substructure, due to contributions at 285 and 285.5 eV, which originates from the three different types of C atoms in coronene. In Figure 3, these C atom types are labeled from 1 to 3. The contributions from type 1 to 3 cannot be distinguished in the NEXAMS spectra. Type 2 contributes to the resonance at 285 eV, and types 1 and 3 contribute to the resonance at 285.5 eV.[19]

The dication spectrum has broader features at 288.5, 290.5, and 293.5 eV. On basis of the NEXAFS studies[14,20,22] on smaller PAHs, we assign the features at 288.5 and 290.5

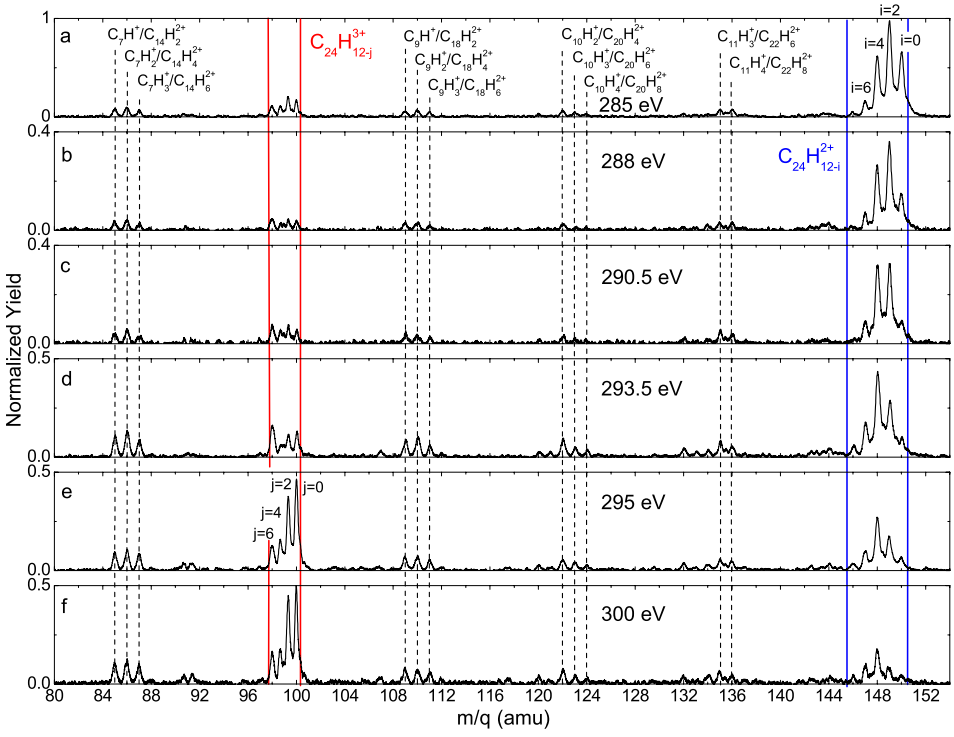

FIG. 2. Normalized mass spectra induced by photons with energies 285, 288, 290.5, 293.5, 295, and 300 eV interacting with coronene cations. The spectra are all normalized to the irradiation time, photon flux, and coronene target intensity. The solid lines indicate the boundaries for the areas leading to the NEXAMS spectra in Figure 3. Note that the trication feature could overlap with monocationic fragments at $\frac{m}{q} = 98$ and 100.

to a mix of higher lying π^* orbitals, σ^* orbitals, and Rydberg states. In earlier studies on coronene[19] and anthracene,[14] the broad feature at 293.5 eV has been assigned to transitions to σ^* orbitals.

The red spectrum in Figure 3 shows NEXAMS data for the trications. The highest yields occur for photon energies exceeding the core ionization threshold. To our knowledge, for $C_{24}H_{12}^+$, the exact value for the core ionization threshold is not known. For neutral $C_{24}H_{12}$, the threshold has been determined at around 290 eV.[21] In Figure 3, the vertical dashed line represents this energy. In our data, we observe a sharp increase of the trication yield at 294 eV. However, the data do not allow for a precise determination of the true core electron binding energy, which is probably a few eV below the clear appearance of trications in our spectra. Below 294 eV, the trication spectrum is very similar to the dication spectrum, i.e., the π^*, σ^*, and Rydberg transitions are clearly observed. This similarity indicates that at these energies, both dications and trications are produced upon the initial resonant K-edge photoexcitation. Below threshold, the ratio between dications and trications is 4:1. Above threshold, the ratio between dication and trication yield is 1:3, which is explained later in part C.

The presence of a significant sub-threshold double ionization channel is not expected from the scheme in Figure 1. There are two possible routes towards this channel: two electron Auger decay and knock-out processes. The emission of two electrons can occur either by Auger Double Ionization (ADI) or by Double Auger Ionization (DAI). In an ADI process, the K-shell vacancy is filled while simultaneously emitting two electrons from the valence levels. In the case of DAI, two subsequent Auger decays take place. This requires that the first Auger decay leaves a deep-lying vacancy in the valence shell which can relax in a subsequent Auger decay.[25] In both cases, a tricationic parent is left

$$M^+ + h\nu \rightarrow M^{+*} \xrightarrow{ADI/DAI} M^{3+*} + 2e^-. \quad (1)$$

Similar double Auger decays have been observed, for instance, for krypton,[23] argon,[24] and carbon monoxide.[25]

An alternative explanation based on regular Auger decay is the knock-out of a weakly bound valence electron by the Auger electron

$$M^+ + h\nu \xrightarrow{\pi^*} M^{+*} \xrightarrow{Auger} M^{2+*} + e^- \xrightarrow{electron\ impact} M^{3+*} + 2e^-. \quad (2)$$

To a certain degree, this process type is comparable to photon double-ionization processes which were recently studied[26] for PAHs. This study revealed double to single ionization ratios of 20%–30% for absorption of 270 eV photons, although, only 5% is attributed to a knock-out mechanism (Ref. 26, Figure 14). The excess energy of the emitted electrons from the valence shell, in that particular case, is in the same range as the energy of the Auger electrons in our experiments, e.g., approximately 220-250 eV.

C. Dehydrogenation and fragmentation dynamics

For a quantitative investigation of dication cooling by H loss, the respective mass spectral features were disentangled by fitting Gaussian line profiles to the spectral features. Highest yields were found for $\frac{m}{q}$ = 147, 148, 149, and 150, associated with 6H, 4H, and 2H loss and intact dications, respectively. The NEXAMS spectra for these processes are displayed in Figure 4. Figure 4(a) shows that formation of intact dications is mainly triggered by C 1s → π^* transitions around 285 eV. Figure 4(b) shows the NEXAMS spectrum associated with 2H loss. This channel is also triggered by the C 1s → π^* transition but occurs also at higher photon energies. The NEXAMS spectrum associated with 4H loss is plotted in Figure 4(c). This channel is triggered by a C 1s → π^* transition around 285 eV and by C 1s → σ^* and Rydberg transitions around 293.5 eV. The loss of 6H (Figure 4(d)) is strongest at energies around 293.5 eV. Similar NEXAMS spectra for the trications are presented in Figure 5. Figures 5(a)–5(c) show a sharp intensity increase at a photon energy of 294 eV, i.e., the threshold energy efficient trication production. Below the threshold, a contribution from the C 1s → π^* transitions around 285 eV does appear in the trication yields (Fig. 5).

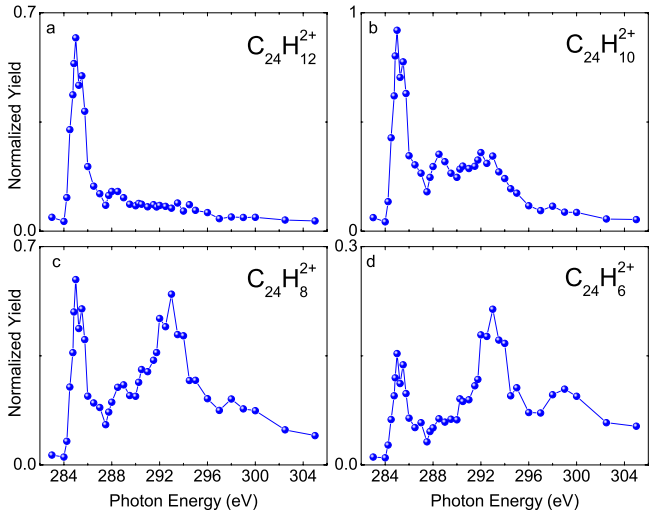

FIG. 4. NEXAMS spectra for $C_{24}H_{12}^{2+}$ (a), $C_{24}H_{10}^{2+}$ (b), $C_{24}H_{8}^{2+}$ (c), and $C_{24}H_{6}^{2+}$ (d), illustrating the strong dependence of the dehydrogenation on the photon energy.

Remarkably, the data reveal that the dication yields for $C_{24}H_{10,8,6}^{2+}$ are non-zero above ionization threshold. Clearly, C 1s ionization followed by an Auger process (Fig. 1(a)) leaves the molecule at least triply charged. The production of dications is either caused by a charge separation process, i.e., H^+ (or H_2^+) loss instead of neutral H (or H_2) loss, or by excitation to shape resonances.[27]

For tricationic coronene, the charge separation process has the form

$$M^{3+*} \longrightarrow [M-H]^{2+*} + H^+ \longrightarrow [M-2H]^{2+*} + H^+ + H \quad (3)$$

or

$$M^{3+*} \longrightarrow [M-2H]^{2+*} + H_2^+. \quad (4)$$

The occurrence of one of these reactions is further supported by the fact that only very little above-threshold formation of $C_{24}H_{12}^{2+}$ is observed (Figure 4(a)). Note that reactions (3) and (4) are conceptually very similar to the superasymmetric fission occurring in multiply charged fullerenes. For C_{60}

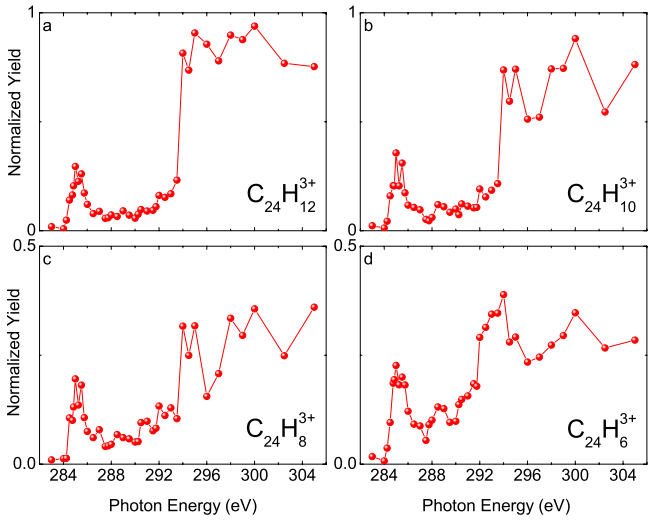

FIG. 5. NEXAMS spectra for $C_{24}H_{12}^{3+}$ (a), $C_{24}H_{10}^{3+}$ (b), $C_{24}H_{8}^{3+}$ (c), and $C_{24}H_{6}^{3+}$ (d).

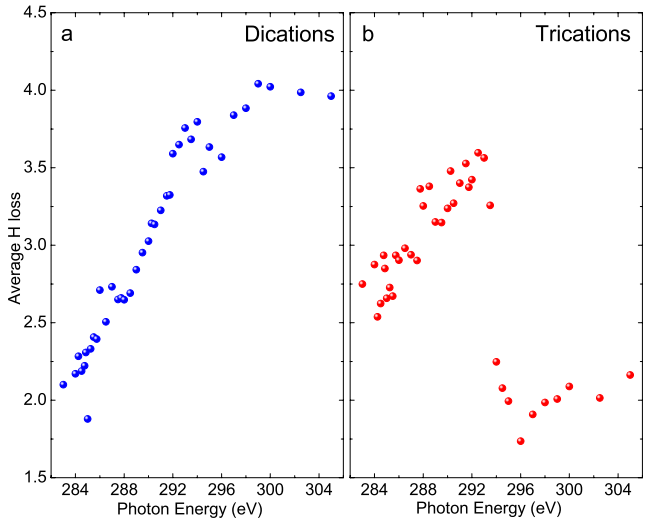

FIG. 6. The average hydrogen loss for dications (a) and tications (b).

charge states exceeding 3+,[28,29] C_2^+ loss becomes dominating over neutral C_2 evaporation. Holm *et al.*[30] have calculated the adiabatic dissociation energies for neutral H atom loss and for H^+ loss from coronene to be 5.2 eV, and 11.4 eV for the monocation, and 4.7 eV and 8.0 eV for the dication, respectively.

Clearly, H^+ loss is thus ruled out for monocations and dications. For the coronene tication, however, the adiabatic dissociation energy for H^+ loss becomes lower than the competing neutral H loss channel.[30] Paris *et al.*[31] have recently investigated hydrogen loss from coronene as a function of charge state, while explicitly including associated energy barriers and considering different spin multiplicities. Their results are qualitatively similar, regarding the transition from neutral H loss to asymmetric fission: starting with the coronene tication, loss of $H^+ + H$ is predicted to be dominant over 2H atom loss. H_2 loss is still dominant over H_2^+ ion loss for tications.

Experimentally, we find the above-threshold ratio between coronene dications and tications, to be 1:3, indicating that charge separation is possible but not yet dominating for triply charged coronene. It has to be noted here that analog to sub-threshold double ionization, there should be a comparable branching ratio for above-threshold triple ionization, leading to formation of intermediate $C_{24}H_{12}^{4+}$. However, this charge state contributes to the tication channel, as for the tetracation, the first hydrogen loss is expected to be solely an asymmetric fission process leading to H^+ or H_2^+ loss.

In the context of dehydrogenation and asymmetric fission, it is interesting to look into the average H loss as a function of photon energy, as this quantity reflects the molecular internal energy *prior* to the breakup process. The average dehydrogenation is defined as $\frac{2I_2+4I_4+6I_6+8I_8}{I_0+I_2+I_4+I_6+I_8}$, in which I_i is the intensity of the peak $C_{24}H_{12-i}^{q+}$. Figure 6 displays the respective data for dications (a) and tications (b). The average dehydrogenation above threshold is ≈4.0 for dications and only ≈2.0 for tications. For tications, H^+ loss leading to dications appears to be more likely to occur in hot tications, whereas neutral H loss is related to internally colder ones. This underlines the notion that the tricationic charge state of coronene marks the opening of the charge separation channel. Neutral H loss, however, still dominates, in particular for modest internal energies. The fact that tications, which are formed above threshold, are internally cold, is well understood using the simple scheme in Figure 1, as the increase in photon energy is entirely transferred to the ejected C 1s electron via direct ionization.

Below the threshold, for dications (Figure 6), a roughly linear increase of average H loss with the photon energy is observed. The increase is a straightforward consequence from the scheme in Figure 1: with increasing photon energy, higher lying unoccupied bound orbitals become resonant, and consequently, the molecular ion is left in a higher excited state. For tications, a similar trend is observed, albeit at slightly higher dehydrogenation states. The above mentioned below-threshold double ionization processes (see Eqs. (1) and (2)) are likely to leave the formed tications with higher excitation energy.

The second possible explanation of dication formation above core ionization threshold is the aforementioned excitation to shape resonances. Such resonances, above ionization threshold, have been observed previously for neutral coronene[19] and benzene.[27] The excitation energy associated with these resonances is higher and consequently should involve stronger dehydrogenation (and even multifragmentation) which is not observed experimentally. We, therefore, conclude that the influence of shape resonances is probably weak for the channels under study.

Clearly, dehydrogenation is the prime fragmentation channel, however, at high energy depositions, PAH skeleton fragmentation becomes relevant. Figure 7 displays NEXAMS spectra of nine PAH fragments which are all formed after breaking the carbon skeleton of coronene. The line color corresponds to the dashed lines in Figure 2. The NEXAMS spectra for smaller fragment cations show strong peaks at 293.5 and 300 eV. Therefore, it is clear that these fragmentation channels are mainly linked to the photoexcitation into the σ^* orbitals. There are two explanations why higher energetic σ^* orbitals are the gateway to these fragments: statistical fragmentation and local bond weakening.

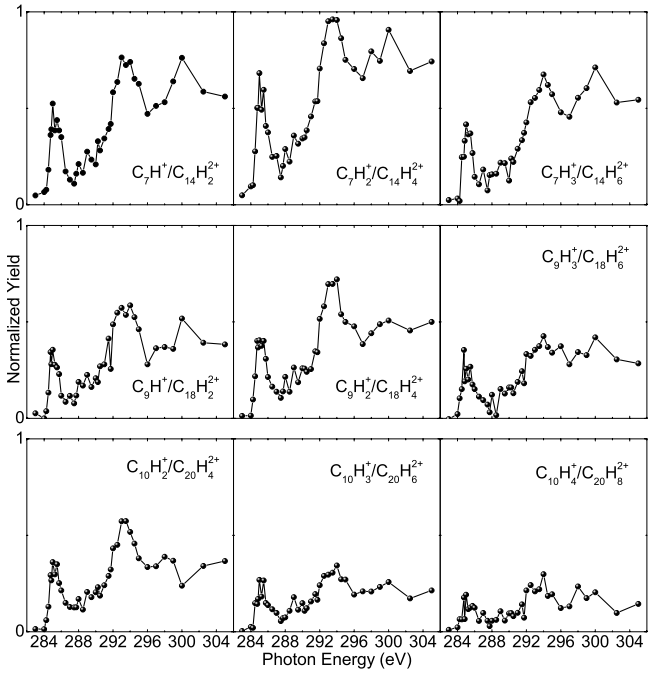

FIG. 7. NEXAMS spectra for fragmentation channels in which the carbon skeleton has been broken.

In statistical fragmentation, the fragmentation depends on the amount of energy which is deposited in the molecule. For core excitation processes, this quantity depends on the binding energy of the associated unoccupied orbital. The energy deposition via the 293.5 eV σ^* orbital is 8.5 eV more than the energy deposition via the 285 eV π^* orbital. The energy deposition which is induced by the subsequent Auger decay remains constant for both excitations. The deposition of higher amounts of energy explains the stronger fragmentation pattern, just below core ionization threshold.

The dominance of σ^* resonances in the fragment NEXAMS spectra can also be explained by a pump-probe type of process. In the first step, a σ bond is weakened by the absorption of a soft X-ray. This bond weakening is rapidly followed by a large energy deposition into the molecule induced by an Auger decay. If the electronic excitation in this particular bond is not yet dissipated to vibrational degrees of freedom when the Auger decay occurs, this type of process can play a role.

D. Evaporation model

Under the assumption that in vibrationally hot PAHs, consecutive H loss competes with infrared (IR) photon emission, one may use a basic cascade model to describe the relaxation of the coronene molecules or PAH molecules in general. The main ingredients for such a model are the infrared photon emission rate, the hydrogen binding energy, and the internal energy. In this scenario, the dissociation probability for dissociation step i can be written as

$$P_i^{diss} = \frac{k_i e^{-E_i/kT_i^{av}}}{\frac{k_{IR}}{n_{max}+1} + k_i e^{-E_i/kT_i^{av}}} \tag{5}$$

with pre-exponential factor $k_i = \frac{kT_i^{eff}}{h} exp\left(1+\frac{\Delta S}{R}\right)$. This expression reflects the dependence of the pre-exponential factors on the entropy change during a reaction at fixed temperature T^{eff}. The average PAH temperature is defined as $T_i^{av} = \sqrt{T_{i,0}^{eff} \times T_{i,n_{max}}^{eff}}$, in which $T_{i,0}^{eff}$ and $T_{i,n_{max}}^{eff}$ correspond to the effective temperatures when 0 or n_{max} infrared photons have been emitted, respectively.[32] In a microcanonical description of a PAH, the effective temperature at step i is defined as

$$T_i^{eff} = 2000\left(\frac{T_{E,i}}{N_C}\right)^{0.4}\left(1-0.2\frac{E_i}{T_{E,i}}\right), \tag{6}$$

in which E_i is the dissociation energy and $T_{E,i}$ is the total vibrational energy at step i.[32] This relation includes a correction for the fact that the heat bath of a PAH is finite. We further set the maximum number of emitted photons $n_{max} = 6$ (Ref. 32) and the entropy change $\Delta S = 2.5$ cal/mol.[33] For coronene, the number of C atoms is $N_C = 24$. Typical IR emission rates are between 1 and 1000 s^{-1}.[8] We adopted $k_{IR} = 10\ s^{-1}$ from Ref. 34. R, h, and k are the gas constant, Planck's constant, and the Boltzmann constant, respectively. We used DFT to determine E_i for atomic and molecular hydrogen loss and the transition states for molecular hydrogen loss. The calculations were performed by using the B3LYP[35,36] functional and a 6-31G(d) basis set as implemented in the GAUSSIAN 09 package.[37] The molecular structures were optimized to a minimum (all real frequencies) or to a transition state (one imaginary frequency) after which the frequencies were calculated. The energies were obtained by subtracting the zero-point energy (corrected by the empirical scaling factor 0.9806 (Ref. 38)) from the total energy. Table I lists all calculated dissociation energies and transition states.

The mass spectra (Figure 2) reveal strong preference for even numbers of H losses over odd numbers of H losses. This suggests that coronene loses hydrogen either by emission of H_2 or by emission of hydrogen pairs. To investigate the competition between H atom loss and H_2 loss, we extended equation (5) as follows:

$$\begin{aligned} P_a^{diss} &= \frac{k_a e^{-E_a/kT_a^{av}}}{\frac{k_{IR}}{n_{max}+1} + k_a e^{-E_a/kT_a^{av}} + k_b e^{-E_b/kT_b^{av}}}, \\ P_b^{diss} &= \frac{k_b e^{-E_b/kT_b^{av}}}{\frac{k_{IR}}{n_{max}+1} + k_a e^{-E_a/kT_a^{av}} + k_b e^{-E_b/kT_b^{av}}}, \\ P^{intact} &= \frac{\frac{k_{IR}}{n_{max}+1}}{\frac{k_{IR}}{n_{max}+1} + k_a e^{-E_a/kT_a^{av}} + k_b e^{-E_b/kT_b^{av}}}. \end{aligned} \tag{7}$$

TABLE I. Calculated adiabatic dissociation energies (for H loss) and energy barriers (for H_2 loss) in eV.

$C_{24}H_{12-(i-1)}^{q+} \rightarrow C_{24}H_{12-i}^{q+} + H$	$E_i^{q=2}$ (eV)	$E_i^{q=3}$ (eV)
$i = 1$	4.7	5.3
$i = 2$	4.2	3.8
$i = 3$	4.7	5.1
$i = 4$	4.0	3.9
$i = 5$	4.9	5.2
$i = 6$	4.0	3.9
$i = 7$	4.8	5.1
$C_{24}H_{12}^{q+} \rightarrow C_{24}H_{10}^{q+} + H_2$	5.2	...

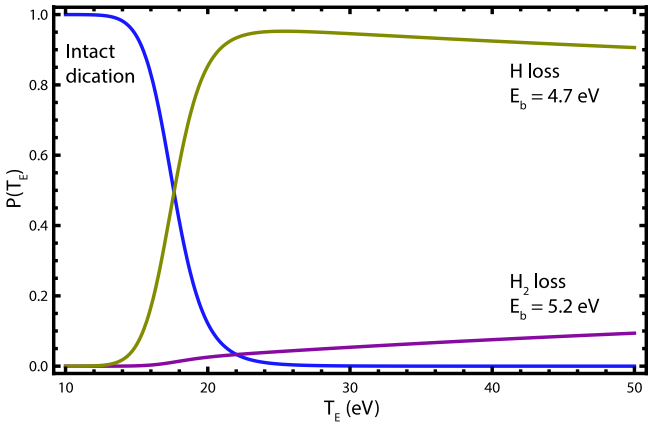

FIG. 8. H atom loss versus H_2 loss from excited coronene dications.

The labels (a) and (b) represent the two competing channels of H atom loss and H_2 loss, respectively. For $C_{24}H_{10}^{2+}$, the respective dissociation energies are $E_a = 4.7$ and $E_b = 5.2$ eV. Figure 8 shows the dissociation probabilities as a function of excitation energy T_E for coronene dications. It is clear that in the relevant energy regime, H atom loss strongly dominates over H_2 loss. Therefore, here H_2 loss is not included in the full cascade model. Only sequential H atom loss is considered.

The dehydrogenation state probability for the ith hydrogen loss is defined as follows:

$$D_i(T_E) = (1 - P_{i+1}^{diss}(T_E)) \prod_{k=0}^{i} P_k^{diss}(T_E). \tag{8}$$

Figure 9 displays $D_i(T_E)$ for i=0-5 as a function of the excitation energy T_E. The loss of even numbers of H atoms clearly dominates over the odd ones, entirely in line with the experimental data (see Figure 2). In order to simulate the mass spectra, an excitation energy distribution has to be implemented in the model.

The branching ratios for the loss channel corresponding to the ith H atom loss A_i can then be determined using

$$A_i = \int D_i(T_E) P(T_E) dT_E. \tag{9}$$

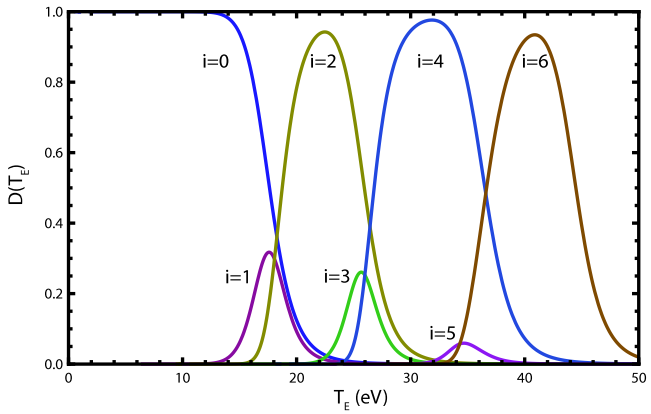

FIG. 9. Dehydrogenation state probabilities of coronene dications, $C_{24}H_{12-i}^{2+}$, as a function of excitation energy T_E.

$P(T_E)$ is the normalized vibrational energy distribution of the system. Under the assumption that the intramolecular vibrational energy redistribution quickly transforms electronic excitation into vibrational energy, it is appropriate to extract an approximation of $P(T_E)$ from an Auger electron spectrum. Because the electronic orbital structure is similar for aromatic hydrocarbons, we use the well-investigated Auger electron spectrum of benzene (Ref. 39, Fig. 7). Typical excitation energies are distributed around 20 eV. The excitation energy depends on the binding energy of the electron pair which is involved in the Auger decay. The lowest amount of energy is deposited when an electron pair residing in the highest occupied molecular orbital is involved. The highest amount of energy is deposited when a 2s electron pair is involved. Note that this reasoning is based on Auger electron emission in a single-electron picture, i.e., all excess energy is released by the emitted electron. In a multi-electron picture, a part of the excess energy is not released by the emitted electron but transferred to excitation of a second electron. In this case, the total amount of excitation energy in the system is higher than would be expected in the single-electron description.

To obtain the excitation energy distribution for the formation of dications by 285 eV photons, 3.7 eV was added to account for the additional excitation energy which is deposited by populating the π^* orbital in the $C(1s) \longrightarrow \pi^*$ transition (Fig. 1). To simulate the mass spectra for other photon energies, the excitation energy distribution was shifted correspondingly. For instance, for 293.5 eV, the excitation energy distribution was up shifted by 8.5 eV with respect to the 285 eV photon case.

For comparison with the experimental data, synthetic spectra were generated by using Gaussian based functions

$$G(x) = \Sigma(A_i + 0.25A_{i-1}) e^{-\frac{(x-\mu_i)^2}{2\sigma^2}} \tag{10}$$

with for μ_i the molecular mass-over-charge ratio and for σ the standard deviation deduced from the experimental peak widths. The term $0.25A_{i-1}$ contains the 20% abundance of one mass unit heavier coronene isotopes present in the target.

Figure 10 compares the experimental dication mass spectra at 285, 288, 290.5, and 293.5 eV photon energies. The simulations show similar trends as the experimental data: a strong preference for even H loss channels and a gentle shift towards higher dehydrogenation with increasing photon energy. However, the loss of 4 and 6H is slightly overestimated in the simulations. Note that the competition of other channels than H atom loss increases with higher degrees of dehydrogenation. These competing processes are not included in the model, possibly leading to an overestimation of higher dehydrogenation states.

The discrepancies between the experimental and model data may be understood by the fact that the values of the relevant parameters are not exactly known for $C_{24}H_{12}^{2+}$. To probe the sensitivity of the model to the parameters, we ran the model for $k_{IR} = 1$, 10, 100 s^{-1} and $n_{max} = 2$, 6, 12 at a 285 eV photon energy. In Figure 11, these model results are presented. The figure shows a rather strong sensitivity for k_{IR}, in particular the intensity of intact $C_{24}H_{12}^{2+}$ (i = 1). The reason for the difference is that a higher IR-emission rate gives faster

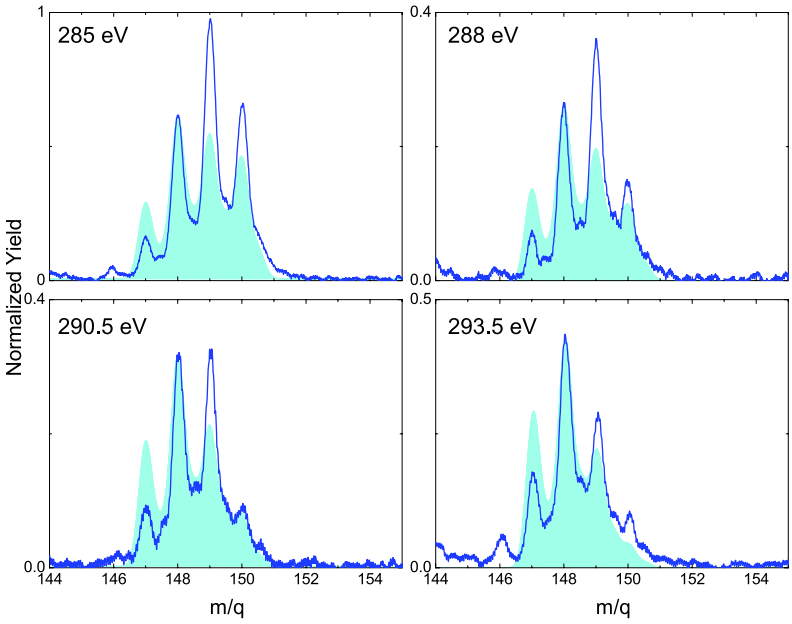

FIG. 10. Zoom-in on the experimental mass spectra (dark blue lines) around the dication feature for photon energies 285, 288, 290.5, and 293.5 eV, compared with simulated mass spectra (light blue).

cooling and thus a higher probability for the fragments to stay intact after a few initial steps of H loss. The model is not very sensitive for changes in n_{max}. The preference for even numbers of H atom loss remains to be pronounced in all cases.

Figure 11 illustrates that modifying the model parameters k_{IR} and n_{max} does not lead to full agreement between the experimental and model data. To exactly reproduce the experimental data with such a cascade model requires a complete

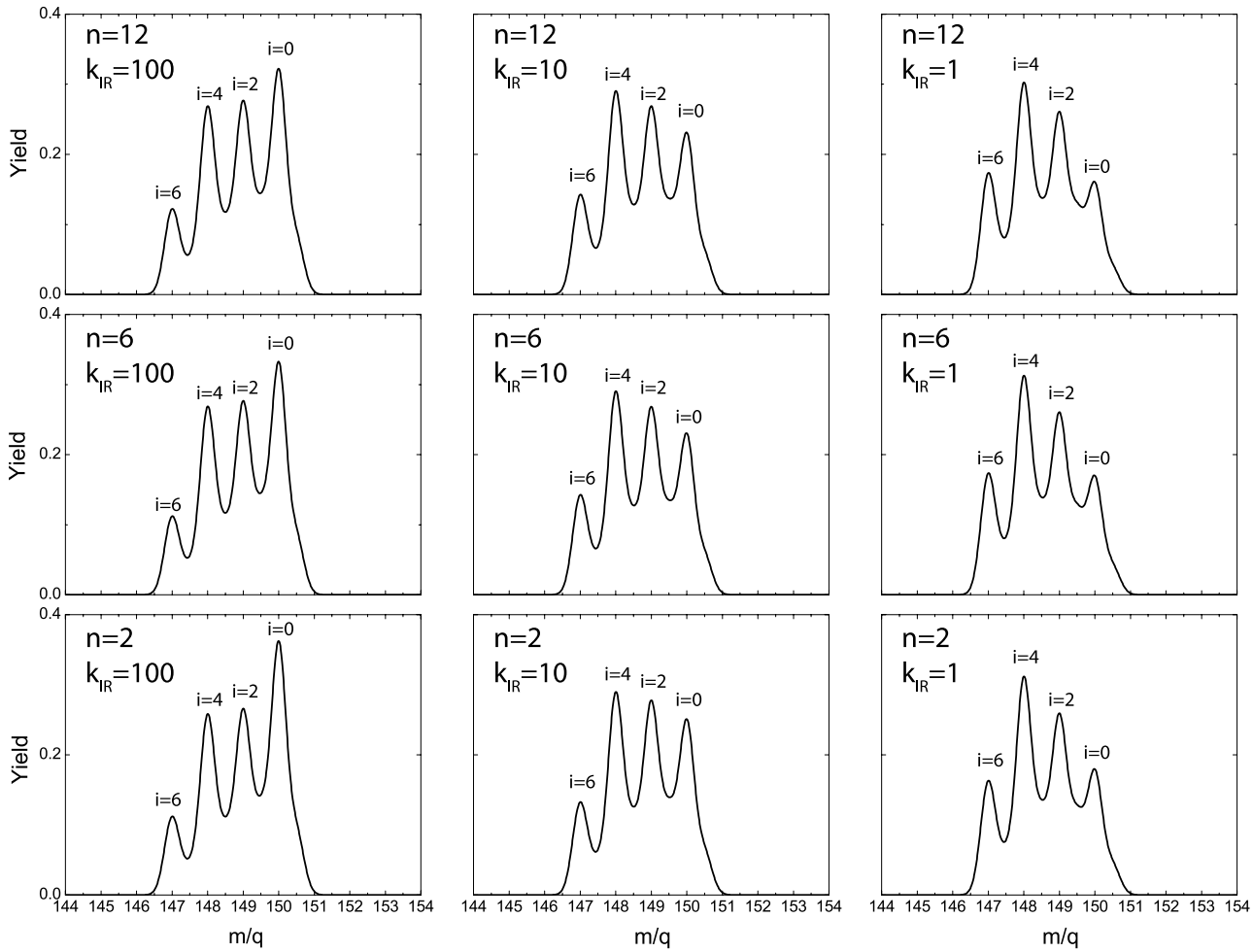

FIG. 11. Model data for different values of the infrared emission rate k_{IR} = 1, 10, 100 s^{-1} and the maximum number of photons n_{max} = 2, 6, 12 with a photon energy of 285 eV. The central panel represents model data for the parameter set used throughout this paper.

investigation of the potential energy surface, including all possible routes towards H atom loss, H_2 loss, and C skeleton break up. Such a theoretical study should also include H atom and H_2 loss pathways via H migration to the PAH surface. For instance, Paris *et al.*[31] performed very advanced calculations which revealed low barrier H_2 loss channels which are in very close competition with H loss, suggesting that contributions from H_2 should be added to such a cascade model. To our knowledge, such advanced theoretical data are not available for multiple H atom and H_2 losses yet.

IV. CONCLUSION

We have investigated the response of gas-phase coronene cations $C_{24}H_{12}^+$ upon soft X-ray photoabsorption around the carbon K-edge. Inner shell excitation or ionization leaves a carbon 1s vacancy, which is subsequently filled in an Auger type process, leading to the formation of intermediate $C_{24}H_{12}^{2+}$ and $C_{24}H_{12}^{3+}$ cations. The Auger mechanism and (below threshold) the excitation into unoccupied molecular orbitals leave these intermediates internally hot, leading to swift de-excitation, predominantly by means of H loss. Density functional theory was employed to determine the dissociation energies for the successive neutral H loss steps. A statistical cascade model based on these dissociation energies was found to reproduce the experimentally obtained dehydrogenation states well. The model is however limited to neutral H or H_2 loss from coronene dications and does not explicitly include charge separation processes, predicted to occur for higher charge states. The experimental data strongly indicate that the intermediate $C_{24}H_{12}^{3+}$ trication is subject to a competition of neutral H loss and asymmetric fission leading to H^+ or loss H_2^+, with the neutral channel dominating and the fission channel being strongest for internally hot parent ions.

ACKNOWLEDGMENTS

We gratefully acknowledge financial support by the Nederlandse organisatie voor Wetenschappelijk Onderzoek (NWO) within the Dutch Astrochemistry Network (DAN). We thank the Helmholtz Zentrum Berlin for allocation of synchrotron beamtime and acknowledge funding from the European Community's Seventh Framework Programme (FP7/2007-2013, Grant No. 312284). We acknowledge support from the European Cost action CM1204 XLIC.

[1]A. G. G. M. Tielens, Annu. Rev. Astron. Astrophys. **46**, 289 (2008).
[2]H. Richter and J. B. Howard, Prog. Energy Combust. Sci. **26**, 565 (2000).
[3]H.-W. Jochims, H. Baumgärtel, and S. Leach, Astrophys. J. **512**, 500 (1999).
[4]F. Qui, Proc. Combust. Inst. **34**, 33 (2013).
[5]E. Rühl, S. D. Price, and S. Leach, J. Phys. Chem. **93**, 6312 (1989).
[6]S. Leach, J. H. D. Eland, and S. D. Price, J. Phys. Chem. **93**, 7575 (1989).
[7]H. W. Jochims, H. Rasekh, E. Rühl, and H. Baumgärtel, Chem. Phys. **168**, 159 (1992).
[8]H. W. Jochims, E. Rühl, H. Baumgärtel, S. Tobita, and S. Leach, Astrophys. J. **420**, 307 (1994).
[9]M. Gatchell, M. H. Stocket, P. Rousseau, T. Chen, K. Kulyk, H. T. Schmidt, J. Y. Chesnel, A. Domaracka, A. Méry, S. Maclot, L. Adoui, K. Støchkel, P. Hvelplund, Y. Wang, M. Alcamí, B. A. Huber, F. Martín, H. Zettergren, and H. Cederquist, Int. J. Mass Spectrom. **365-366**, 260-265 (2014).
[10]M. H. Stockett, H. Zettergren, L. Adoui, J. D. Alexander, U. Bērziņš, T. Chen, M. Gatchell, N. Haag, B. A. Huber, P. Hvelplund, A. Johansson, H. A. B. Hohansson, K. Kulyk, S. Rosén, P. Rousseau, K. Støchkel, H. T. Schmidt, and H. Cederquist, Phys. Rev. A **89**, 032701 (2014).
[11]J. Postma, R. Hoekstra, A. G. G. M. Tielens, and T. Schlathölter, Astrophys. J. **783**, 61 (2014).
[12]G. Malloci, G. Mulas, and C. Joblin, Astron. Astrophys. **426**, 105 (2004).
[13]D. Hübner, F. Holch, M. L. M. Rocco, K. C. Prince, S. Stranges, A. Schöll, E. Umbach, and R. Fink, Chem. Phys. Lett. **415**, 188 (2005).
[14]M. Klues, K. Hermann, and G. Witte, J. Chem. Phys. **140**, 014302 (2014).
[15]A. R. Milosavljevic, C. Nicolas, J. Lemaire, C. Dehon, R. Thissen, J.-M. Bizau, M. Réfrégiers, L. Nahon, and A. Giuliani, Phys. Chem. Chem. Phys. **13**, 15432 (2011).
[16]S. Bari, O. Gonzalez-Magaña, G. Reitsma, J. Werner, S. Schippers, R. Hoekstra, and T. Schlathölter, J. Chem. Phys. **134**, 024314 (2011).
[17]G. Reitsma, H. Zettergren, L. Boschman, E. Bodewits, R. Hoekstra, and T. Schlathölter, J. Phys. B: At., Mol. Opt. Phys. **46**, 245201 (2013).
[18]G. Reitsma, L. Boschman, M. J. Deuzeman, O. Gonzalez-Magaña, S. Hoekstra, S. Cazaux, R. Hoekstra, and T. Schlathölter, Phys. Rev. Lett. **113**, 053002 (2014).
[19]H. Oji, R. Mitsumoto, E. Ito, H. Ishii, Y. Ouchi, K. Seki, T. Yokoyama, T. Ohta, and N. Kosugi, J. Chem. Phys. **109**, 10409 (1998).
[20]C. Kolczewski, R. Püttner, M. Martins, A. S. Schlachter, G. Snell, M. M. Sant'Anna, K. Hermann, and G. Kaindl, J. Chem. Phys. **124**, 034302 (2006).
[21]G. Fronzoni, O. Baseggio, M. Stener, W. Hua, G. Tian, Y. Luo, B. Apicella, M. Alfé, M. de Simone, A. Kivimäki, and M. Coreno, J. Chem. Phys. **141**, 044313 (2014).
[22]R. Püttner, C. Kolczewski, M. Martins, A. S. Schlachter, G. Snell, M. Sant'Anna, J. Viefhaus, K. Hermann, and G. Kaindl, Chem. Phys. Lett. **393**, 361-366 (2004).
[23]S. Sheinerman, P. Linusson, J. H. D. Eland, L. Hedin, E. Andersson, J.-E. Rubensson, L. Karlsson, and R. Feifel, Phys. Rev. A **86**, 022515 (2012).
[24]J. Zeng, P. Liu, W. Xiang, and J. Yuan, Phys. Rev. A **87**, 033419 (2013).
[25]L. Journel, R. Guillemin, A. Haouas, P. Lablanquie, F. Penent, J. Paloudoux, L. Andric, M. Simon, D. Céolin, T. Kaneyasu, J. Viefhaus, M. Braune, W. B. Li, C. Elkharrat, F. Catoire, J.-C. Houver, and D. Dowek, Phys. Rev. A **77**, 042710 (2008).
[26]T. Hartman, P. N. Juranić, K. Collins, B. Reilly, E. Makoutz, N. Appathurai, and R. Wehlitz, Phys. Rev. A **87**, 063403 (2013).
[27]E. E. Rennie, B. Kempgens, H. M. Köppe, U. Hergenhahn, J. Feldhaus, B. S. Itchkawitz, A. L. D. Kilcoyne, A. Kivimäki, K. Maier, M. N. Piancastelli, M. Polcik, A. Rüdel, and A. M. Bradshaw, J. Chem. Phys. **113**, 7362 (2000).
[28]P. Scheier, B. Dünser, and T. D. Märk, Phys. Rev. Lett. **74**, 3368 (1995).
[29]H. Cederquist, J. Jensen, H. T. Schmidt, H. Zettergren, S. Tomita, B. A. Huber, and B. Manil, Phys. Rev. A **67**, 062719 (2003).
[30]A. I. S. Holm, H. A. B. Johansson, H. Cederquist, and H. Zettergren, J. Chem. Phys. **134**, 044301 (2011).
[31]C. Paris, M. Alcamí, F. Martín, and S. Díaz-Tendero, J. Chem. Phys. **140**, 204307 (2014).
[32]E. R. Micelotta, A. P. Jones, and A. G. G. M. Tielens, Astron. Astrophys. **510**, A37 (2010).
[33]Y. Ling and C. Lifshitz, J. Phys. Chem. A **102**, 708 (1998).
[34]R. C. Dunbar, J. H. Chen, H. Y. So, and B. Asamoto, J. Chem. Phys. **86**, 2081-2086 (1987).
[35]A. D. Becke, J. Chem. Phys. **98**, 5648 (1993).
[36]C. Lee, W. Yang, and R. G. Parr, Phys. Rev. B **37**, 785 (1988).
[37]M. J. Frisch *et al.*, GAUSSIAN 09, Gaussian, Inc., Wallingford, CT (2009).
[38]A. P. Scott and L. Radom, J. Phys. Chem. **100**, 16502-16513 (1996).
[39]R. R. Rye and J. E. Houston, Acc. Chem. Res. **17**, 41-47 (1984).